

**Theoretical study of the three-dimensional quantum Hall effect in a periodic electron system**H. Geng<sup>1,2</sup>, G. Y. Qi,<sup>1</sup> L. Sheng,<sup>1,2,\*</sup> W. Chen,<sup>1,2,†</sup> and D. Y. Xing<sup>1,2</sup><sup>1</sup>*National Laboratory of Solid State Microstructures and Department of Physics, Nanjing University, Nanjing 210093, China*<sup>2</sup>*Collaborative Innovation Center of Advanced Microstructures, Nanjing University, Nanjing 210093, China*

(Received 10 May 2021; revised 26 September 2021; accepted 28 October 2021; published 15 November 2021)

The existence of a three-dimensional quantum Hall effect (3D QHE) due to spontaneous Fermi surface instabilities in strong magnetic fields was proposed decades ago, and has stimulated recent progress in experiments. The reports in recent experiments show that the Hall plateaus and vanishing transverse magnetoresistivities (TMRs) (which are two main signatures of 3D QHE) are not easily observed in natural materials. Two main explanations for the slowly varying slopelike Hall plateaus and nonvanishing TMRs [which can be referred to as the quasiquantized Hall effect (QQHE)] have been proposed. By studying the magnetotransport with a simple effective periodic 3D system, we show how 3D QHE can be achieved in certain parameter regimes. We find two mechanisms that may give rise to QQHE. One mechanism is the “low” Fermi energy effect, and the other is the “strong” impurity effect. Our studies also prove that an artificial superlattice is an ideal platform for realizing 3D QHE with a high layer barrier periodic potential.

DOI: [10.1103/PhysRevB.104.205305](https://doi.org/10.1103/PhysRevB.104.205305)**I. INTRODUCTION**

The discoveries of quantum Hall effects (QHEs) [1–3] in two-dimensional (2D) electron gas have inspired the discovery and classification of topological materials in condensed-matter physics [4–6]. The main feature of 2D QHE is that the quantized Hall conductivities take values  $\sigma_{xy} = \nu e^2/h$ , with  $\nu$  the integers and transverse magnetoconductivities (TMCs)  $\sigma_{\alpha\alpha}$  or transverse magnetoresistivities (TMRs)  $\rho_{\alpha\alpha}$  with  $\alpha = x, y$  disappearing when the Hall plateaus appear. Here, “transverse” means perpendicular to the direction of the magnetic field, e.g., the  $z$  direction. Another important feature of 2D QHE is the formation of dissipationless one-dimensional (1D) chiral edge states protected by topology [7]. Similar effects have been discovered in quasi-2D systems with stacking 2D QHE layers where the interlayer coupling is much weaker than the Landau level (LL) spacing [8–12]. These quasi-2D QHEs have a similar quantized Hall conductance  $G_{xy} = \nu e^2/h$  which can be regarded as 2D QHE in quasi-2D systems. In contrast to 2D and quasi-2D electron gas systems, the QHE was thought to be forbidden in three-dimensional (3D) electron gas. The reason is that the third dimension, along the direction of the magnetic field, spreads the LLs into overlapping bands, thereby no energy gap exists between the LLs, and the band quantization is destroyed. But the discoveries of 3D topological systems offer a possible way to realize QHE. The key point is that some 3D topological systems may have topologically protected 2D electron gas at the surfaces [4,6] which can give rise to 2D QHE [13–16]. This may also result in quantized Hall conductance just as quasi-2D systems.

Despite the search for quantized Hall conductances in quasi-2D systems or topological 3D systems, searches have

been conducted for quantized Hall conductivities in bulk 3D systems. In fact, in the vicinity of the quantum limit, 3D electron systems also tend to form varieties of correlated electron states [17], including Luttinger liquids, charge density waves (CDWs), spin density waves (SDWs), valley density waves (VDWs), excitonic insulators, Wigner crystals, Hall crystals, and staging transitions in the case of highly anisotropic layered systems [17–23]. It has been predicted that 3D QHE could be observed in semimetals and doped semiconductors [17,24–26]. In these systems, the application of a magnetic field would lead to Fermi surface instability, which may cause a periodic modulation of the electron density such as CDWs, or SDW along the direction of the magnetic field. From this point, signatures of 3D QHE are also manifestations of the emergence of correlated states. The main distinct signature of 3D QHE is the value of Hall conductivity plateaus  $\sigma_{xy} = G_z e^2/2\pi h$  which are different from 2D QHE, where  $G_z$  is the  $z$  component of a reciprocal (super)lattice vector or the period of the  $z$  direct potential. The 3D QHE is also expected to have the same signature of vanishing TMCs, namely  $\sigma_{xx} = 0$ . The dissipationless edge states in 3D QHE systems perform differently compared with the edge states in 2D QHE systems. The surface parallel to the magnetic field may carry surface states that are dissipationless along the transverse direction but diffusive along the longitudinal  $z$  direction [27,28].

Inspired by these ideas, signatures of 3D QHE have been reported to be observed in several systems. Decades ago, the bulk QHE was observed in fabricated artificial superlattices [29]. Even though it is not a strict 3D QHE as the Hall resistivities are still dependent on the thickness of the systems rather than depending on the thickness of only one layer of the superlattice, it is still a good example that demonstrates the existence of a periodic potential will open gaps in the overlapping LLs. We can expect that when the thickness of the superlattice is large enough, a true 3D QHE may appear. On the other hand, spontaneous mechanisms to arrive at 3D

\* shengli@nju.edu.cn

† pchenweis@gmail.com

QHE systems were proposed theoretically decades ago, but this phenomenon has not been observed experimentally until recently [30–32] in the semimetal systems of bulk ZrTe<sub>5</sub> and HfTe<sub>5</sub>. The 3D QHE observed in experiment [30] is carefully explained by the CDW mechanism [33]. Particularly, the Hall resistivity  $\rho_{xy}$  has been found to exhibit a plateau with a value of  $h\pi/e^2k_F$  which is consistent with the CDW mechanism. This is because the Fermi surface instability leads to the formation of a CDW with a wavelength of half of the Fermi wavelength, and specifically, the period of the CDW is  $Z_{CDW} = \pi/k_F$ . However, the other signatures of 3D QHE, vanishing TMCs, were only reported to be observed in Ref. [30]. In other papers, TMCs (TMRs) are minimum finite values, and it was speculated that possibly other Fermi pockets near the Fermi surface may lead to this [31]. Very recently, another group [34] also investigated the physics of ZrTe<sub>5</sub> in a magnetic field. They claimed that they observed the so-called quasiquantized Hall effect (QQHE) in ZrTe<sub>5</sub> systems. The main difference between QQHE and 3D QHE is that in QQHE, the quasiquantized Hall plateaus appear with nonvanishing TMCs (or TMRs) rather than vanishing ones. Above all, it seems that the transport signatures of 3D QHE in electron systems with a periodic potential are rather complex. It is necessary to theoretically study the TMCs (or TMRs) and Hall conductivities (or resistivities) in detail and give more insight into this phenomenon.

In this paper, we effectively model these periodic systems with a periodic square-well potential along the  $z$  direction which is usually known as the Kronig-Penney model. Then, a magnetic field along the  $z$  direction is applied in the system. We explicitly calculate the energy bands, density of states (DOS), and Hall conductivities without impurities. From these results, the origin of 3D QHE can be clearly understood by the origin of the gaps from the periodic potential. To compare with experimental results, impurities are taken into consideration, and we studied the TMRs  $\rho_{xx}$  and Hall resistivities  $\rho_{xy}$ . Our results show that quantized Hall resistivities  $\rho_{xy}$  and vanishing TMRs  $\rho_{xx}$  are surely a signature of the appearance of 3D QHE in periodic systems. In addition, we find that even results with slopelike quasiquantized Hall resistivities with finite TMRs (which we refer to as QQHE in this paper) in the vicinity of the quantum limit can have other origins despite the reasons mentioned in Refs. [31,34]. We find that “low” Fermi energies and “strong” impurities may give rise to QQHE in periodic potential electron systems. We cannot just conclude whether a periodic potential exists from QQHE observations. Finally, the advantage of the artificial superlattice is also discussed.

This paper is arranged as follows. In Sec. II, the general model and methods are presented. In Sec. III, the Kronig-Penney model for a periodic potential along the  $z$  direction is considered, and the main results will be presented. In Sec. IV, a discussion of the results and a conclusion will be made.

## II. MODEL AND METHODS

To model the periodic system made by a superlattice or modulated periodic potential, let us consider a cuboid 3D normal metal system with a length, width, and height of  $L_x$ ,  $L_y$ , and  $L_z$ , respectively. The Hamiltonian, including the

vector potential  $\mathbf{A}$ , modulation periodic potential  $V(z)$  satisfying  $V(z+Z) = V(z)$ , and random potential  $U(\mathbf{r})$ , can be described as

$$H = H_0 + U(\mathbf{r}), \quad (1)$$

where  $H_0 = \frac{\mathbf{p}^2}{2M} + V(z)$  is the Hamiltonian of a free electron in the magnetic field with the mechanical momenta  $\mathbf{P} = \mathbf{p} + e\mathbf{A}$ , where  $M$  is the effective mass assumed isotropic and the canonical momenta  $\mathbf{p} = -i\hbar\nabla$ . Although what we are considering is a rough and simple approximation, it is enough to give some insight into the real systems.

### A. Landau levels and quantized Hall conductivities

Applying the magnetic field along the  $z$  direction, namely,  $\mathbf{B} = (0, 0, B)$ , and choosing the vector potential within the Landau gauge as  $\mathbf{A} = (0, Bx, 0)$ , we can write down the basic commutation relations for the coordinate and momentum operators,  $[P_x, P_y] = -ie\hbar B$  and  $[\mathbf{P}, f(\mathbf{r})] = -i\hbar\nabla f(\mathbf{r})$ , where  $f(\mathbf{r})$  is a function of coordinate  $\mathbf{r}$ . The velocity operator can be obtained as  $\mathbf{v} = \nabla_{\mathbf{P}}H = \frac{\mathbf{p}}{M}$ . The stationary Schrödinger equation of  $H_0$  is

$$H_0|\Psi\rangle = E|\Psi\rangle. \quad (2)$$

One way to solve this problem is to introduce the ladder operators  $a$  and  $a^+$  with the commutation relation  $[a, a^+] = 1$ . Then the components of mechanical momentum can be expressed as  $P_x = \frac{\hbar}{\sqrt{2}l_B}(a + a^+)$  and  $P_y = \frac{i\hbar}{\sqrt{2}l_B}(a - a^+)$ , where  $l_B = \sqrt{\frac{\hbar}{eB}}$  is the magnetic length. Similarly, the velocity operators are

$$\begin{aligned} \hat{v}_x &= \frac{\hbar}{\sqrt{2}Ml_B}(a + a^+), \\ \hat{v}_y &= \frac{i\hbar}{\sqrt{2}Ml_B}(a - a^+). \end{aligned} \quad (3)$$

The Hamiltonian  $H_0$  is expressed in terms of ladder operators as

$$H_0 = \hbar\omega_c\left(a^+a + \frac{1}{2}\right) + \frac{p_z^2}{2M} + V(z), \quad (4)$$

where  $\omega_c = \frac{eB}{M}$  is the cyclotron frequency. As can be easily seen from Eq. (4),  $H_0$  can be divided into two independent parts  $h^{\parallel}$  and  $h^{\perp}$ , which are

$$h^{\parallel} = \frac{p_z^2}{2M} + V(z) \quad (5)$$

and

$$h^{\perp} = \hbar\omega_c\left(a^+a + \frac{1}{2}\right). \quad (6)$$

Therefore, we can obtain the eigenstates of  $h^{\parallel}$  and  $h^{\perp}$ , respectively, and the eigenstates of  $H_0$  are just given by them. From the standard quantum mechanics textbook, e.g., Ref. [35], the eigenstate of  $h^{\perp}$  can be represented by two quantum numbers: the LL  $N$  and the guiding center  $X$ , which are the eigenvalues of  $a^+a$  and  $-\frac{l_B^2}{\hbar}p_y$ . The eigenstate of  $h^{\parallel}$  is merely one-dimensional Bloch waves, which can also be denoted by two quantum numbers, the Bloch band number  $n_b$  and the quasiwavenumber  $k_z$ . The allowed values that can be taken by

these quantum numbers are  $N \in \{0, 1, 2, \dots\}$ ,  $X \in \{x|0 < x < L_x\}$ ,  $n_b \in \{1, 2, 3, \dots\}$ , and  $k_z \in \{k_z|-\frac{\pi}{Z} < k_z < \frac{\pi}{Z}\}$ .

Denoting the complete set of quantum numbers as  $\gamma = (N, X, n_b, k_z)$  for convenience, we can acquire the eigensolution of  $H_0$ : The eigenstate can be formally marked as  $|\gamma\rangle$  and the corresponding eigenenergy is

$$E_\gamma = (N + \frac{1}{2})\hbar\omega_c + E_{n_b, k_z}. \quad (7)$$

In this eigenbasis, the velocity operators can be represented as

$$\begin{aligned} \hat{v}_{\gamma, \gamma'}^x &= \frac{\hbar\delta_{\bar{\gamma}, \bar{\gamma}'}}{\sqrt{2}Ml_B} (\sqrt{N+1}\delta_{N+1, N'} + \sqrt{N'}+1\delta_{N, N'+1}), \\ \hat{v}_{\gamma, \gamma'}^y &= \frac{i\hbar\delta_{\bar{\gamma}, \bar{\gamma}'}}{\sqrt{2}Ml_B} (\sqrt{N+1}\delta_{N+1, N'} - \sqrt{N'}+1\delta_{N, N'+1}), \end{aligned} \quad (8)$$

where  $\bar{\gamma} = (X, n_b, k_z)$ , and we use the relations  $a^+|N, \bar{\gamma}\rangle = \sqrt{N+1}|N+1, \bar{\gamma}\rangle$ ,  $a|N, \bar{\gamma}\rangle = \sqrt{N}|N-1, \bar{\gamma}\rangle$ , and  $\langle N, \bar{\gamma}|N', \bar{\gamma}'\rangle = \delta_{N, N'}\delta_{\bar{\gamma}, \bar{\gamma}'}$ . To obtain the Hall conductivity, we mainly use the Kubo-Greenwood formula which can be formally expressed as [36,37]

$$\sigma_{ij} = -\frac{ig_s e^2 \hbar}{\Omega} \sum_{\varepsilon_\alpha \neq \varepsilon_\beta} \frac{f(\varepsilon_\alpha) - f(\varepsilon_\beta)}{\varepsilon_\alpha - \varepsilon_\beta} \frac{\langle \alpha | \hat{v}_i | \beta \rangle \langle \beta | \hat{v}_j | \alpha \rangle}{\varepsilon_\alpha - \varepsilon_\beta - \hbar\omega + i\eta}, \quad (9)$$

where  $\varepsilon_\alpha$  and  $\varepsilon_\beta$  are the eigenenergies corresponding to the eigenstates  $|\alpha\rangle$  and  $|\beta\rangle$  of the system, respectively, and  $g_s$  is a degeneracy factor.  $\Omega = L_x L_y L_z$  is the volume of the system.  $f(\varepsilon_\alpha)$  and  $f(\varepsilon_\beta)$  are the Fermi-Dirac distribution functions, defined as  $f(x) = 1/[e^{(x-E_F)/k_B T} + 1]$ , where  $E_F$  is the Fermi energy of the system.  $\hat{v}_i$  and  $\hat{v}_j$  are the velocity operators and  $\eta$  is the small positive value which can be regarded as the self-energy arising from defects.

For the Hall conductivities at zero temperature, namely,  $\omega \rightarrow 0$ , and for a clean system,  $\eta \rightarrow 0^+$ , Eq. (9) can be further simplified as

$$\sigma_{xy} = \frac{2g_s e^2 \hbar}{\Omega} \sum_{N, N', \bar{\gamma}} \frac{\text{Im}[\langle N', \bar{\gamma} | \hat{v}_x | N, \bar{\gamma} \rangle \langle N, \bar{\gamma} | \hat{v}_y | N', \bar{\gamma} \rangle]}{(E_{N', \bar{\gamma}} - E_{N, \bar{\gamma}})^2}, \quad (10)$$

where  $E_{N', \bar{\gamma}} < E_F < E_{N, \bar{\gamma}}$ , and  $\text{Im}[c]$  is taking the imaginary part of some complex number  $c$ . First, we substitute the matrix elements of the velocities in Eq. (8) into Eq. (10). Second, for the same  $\bar{\gamma}$ , the eigenenergies only differ by the energy of the Landau levels. That is,  $E_{N', \bar{\gamma}} - E_{N, \bar{\gamma}} = E_{N', X}^\perp - E_{N, X}^\perp = (N' - N)\hbar\omega_c$ . Third, the degeneracy of LLs is  $\sum_X 1 = \frac{L_x L_y}{2\pi l_B^2}$ . Finally, with a periodic boundary condition in the  $z$  direction,  $\sum_{k_z} \dots \rightarrow \frac{L_z}{2\pi} \int dk_z \dots$ . Finally, we get the expression for the Hall conductivity,

$$\sigma_{xy} = g_s \frac{e^2}{2\pi\hbar} \left( \sum_{N, n_b} \int_{E < E_F} 1 dk_z \right). \quad (11)$$

By taking  $g_s = 1$  for the nondegeneracy case, the result is consistent with Halperin's result [17].

To get a stable 3D QHE from the system, the gap of Landau levels should be large enough, so that the first Landau level Bloch band should be larger than the zeroth Landau level first Bloch band, or  $E(N=0, X, n_b=1, k_z=\pm\pi/Z) < E(N=1, X, n_b=1, k_z=0)$ , which also means that the gap of the

nearest Landau levels is larger than the energy difference in the first Bloch bands. In this case, there will be at least one stable quantized Hall plateau.

## B. Impurities, level broadening, and magnetoconductivities

To gain a further understanding of the 3D QHE system, we need to obtain the vanishing TMCs accompanied by the Hall plateaus. For the transverse electronic transport, namely,  $\mathbf{E} \perp \mathbf{B}$ , noticing that the LLs do not disperse along the  $x$  or  $y$  direction from Eq. (7), the electrons described by the Hamiltonian  $H_0$  cannot drift in the  $x$ - $y$  plane. More specifically, we look back to Eq. (9) and simplify it by taking the subscripts  $j = i$  with  $\hbar\omega \rightarrow 0$ , so

$$\sigma_{ii} = -\frac{\pi g_s e^2 \hbar}{\Omega} \sum_{\varepsilon_\alpha \neq \varepsilon_\beta} \frac{\partial f(\varepsilon_\alpha)}{\partial \varepsilon_\alpha} \delta(\varepsilon_\alpha - \varepsilon_\beta) |\langle \alpha | \hat{v}_i | \alpha \rangle|^2. \quad (12)$$

Combining Eq. (12) with Eq. (8), we can see that the diagonal elements of the velocity terms of  $i = x$  and  $i = y$  will vanish without impurities.

It is time that we pull in the random potential  $U(\mathbf{r})$  induced by impurities and defects. Let us consider a randomly distributed potential

$$U(\mathbf{r}) = \sum_{i=1}^{N_{\text{imp}}} U_i u(\mathbf{r} - \mathbf{R}_i), \quad (13)$$

where  $U_i$  follows a binomial distribution with equal probability to choose a value of  $-W$  or  $W$ ,  $\mathbf{R}_i$  is uniform randomly distributed in the volume  $\Omega$ , and  $N_{\text{imp}}$  is the number of impurities.

For the static case  $\omega \rightarrow 0$ , a convenient derivation of the Kubo-Greenwood formula is the so-called Kubo-Bastin formalism [38]. Taking into account that  $\lim_{\eta \rightarrow 0^+} \frac{1}{(\varepsilon_\alpha - \varepsilon)(\varepsilon_\alpha - \varepsilon + i\eta)} = \lim_{\eta \rightarrow 0^+} \frac{d}{d\varepsilon} \left\{ \frac{1}{\varepsilon_\alpha - \varepsilon + i\eta} \right\}$ , Eq. (9) can be written as [37]

$$\begin{aligned} \sigma_{ij} &= -\frac{g_s e^2 \hbar}{2\pi\Omega} \int d\varepsilon f_F(\varepsilon) \\ &\times \text{Tr} \left[ \hat{v}_i \frac{\partial G_\varepsilon^+}{\partial \varepsilon} \hat{v}_j \Delta G_\varepsilon - \hat{v}_i \Delta G_\varepsilon \hat{v}_j \frac{\partial G_\varepsilon^-}{\partial \varepsilon} \right], \end{aligned} \quad (14)$$

where we have used the definitions  $\text{Tr}[\hat{O}]$  taking the trace of the operator matrix  $\hat{O}$ , and the one-body Green's function  $G(z) = \frac{1}{z-H}$ , and also the relations [39]  $\delta(\lambda - H) = -\frac{1}{2\pi i} \Delta G_\lambda = \mp \frac{1}{\pi} \text{Im} G_\lambda^\pm$ ,  $\Delta G_\lambda = (G_\lambda^+ - G_\lambda^-)$ , and  $G_\lambda^\pm = G(\lambda \pm i0^+)$ , with  $\lambda$  being a real number. Macroscopic physical quantities, e.g., transport conductivities, are associated with averaged characteristics over the distribution of impurities. For this reason, the conductivities introduced by Eq. (14) must be averaged,

$$\begin{aligned} \sigma_{ij} &= -\frac{g_s e^2 \hbar}{2\pi\Omega} \int d\varepsilon f_F(\varepsilon) \\ &\times \left\langle \left\langle \text{Tr} \left[ \hat{v}_i \frac{\partial G_\varepsilon^+}{\partial \varepsilon} \hat{v}_j \Delta G_\varepsilon - \hat{v}_i \Delta G_\varepsilon \hat{v}_j \frac{\partial G_\varepsilon^-}{\partial \varepsilon} \right] \right\rangle \right\rangle, \end{aligned} \quad (15)$$

where  $\langle \langle \dots \rangle \rangle$  means taking the average over the random potential.

Assuming  $j = i$ , a more simple form of Eq. (15) is obtained for the diagonal conductivity tensor [40],

$$\sigma_{ii} = -g_s \frac{e^2 \hbar}{4\pi \Omega} \int d\varepsilon \left( -\frac{\partial f(\varepsilon)}{\partial \varepsilon} \right) \times \langle \langle \text{Tr}[\hat{v}_i \Delta G_\varepsilon \hat{v}_i \Delta G_\varepsilon] \rangle \rangle. \quad (16)$$

The averaged Green's function  $G_\varepsilon^s$  (with  $s = \pm$ ) of the electron interacting with a random scattering potential has only nonzero diagonal elements in the LL representation. This can be expressed as

$$\langle \langle X G_\varepsilon^s(\gamma, \gamma') \rangle \rangle = G_\varepsilon^s(\gamma) \delta_{\gamma, \gamma'}. \quad (17)$$

Below we consider the limit of the short-range scattering potential, and neglect the vertex correction to the correlation functions in Eq. (15). Combining Eqs. (14), (15), and (8), we obtain TMC,

$$\sigma_{xx} = g_s \frac{e^2 (\hbar \omega_c)^2}{4\pi^2 \hbar} \int d\varepsilon \left( -\frac{\partial f}{\partial \varepsilon} \right) \int dk_z \sum_{N, n_b} (N+1) \times \text{Re}[G_\varepsilon^-(n_b, k_z, N) \Delta G_\varepsilon(n_b, k_z, N+1)], \quad (18)$$

and the Hall conductivity,

$$\begin{aligned} \sigma_{xy} = & g_s \frac{e^2 (\hbar \omega_c)^2}{4\pi^2 \hbar} \int d\varepsilon \int dk_z \sum_{N=0}^{\infty} \sum_{n_b} (N+1) \\ & \times \text{Im} \left[ \frac{\partial f}{\partial \varepsilon} G_\varepsilon^-(n_b, k_z, N) G_\varepsilon^+(n_b, k_z, N+1) \right. \\ & + f(\varepsilon) \left( G_\varepsilon^+(n_b, k_z, N) \frac{\partial G_\varepsilon^+(n_b, k_z, N+1)}{\partial \varepsilon} \right. \\ & \left. \left. - \frac{\partial G_\varepsilon^+(n_b, k_z, N)}{\partial \varepsilon} G_\varepsilon^+(n_b, k_z, N) \right) \right]. \quad (19) \end{aligned}$$

In the self-consistent Born approximation (SCBA) [40–42], we get

$$\Sigma_\varepsilon^s(\gamma) = \sum_{\gamma'} \langle \langle |U_{\gamma', \gamma}|^2 \rangle \rangle G_\varepsilon^s(\gamma'), \quad (20)$$

with

$$G_\varepsilon^s(\gamma) = [\varepsilon - E_\gamma - \Sigma_\varepsilon^s(\gamma)]^{-1}. \quad (21)$$

Here,  $U_{\gamma', \gamma} = \langle \gamma' | U | \gamma \rangle$  are the matrix elements of the potential  $U$  in the  $H_0$  eigenbasis. Let us transform the impurity potential into Fourier series according to the standard relations

$$\begin{aligned} u(\mathbf{r}) &= \frac{1}{\Omega} \sum_{\mathbf{q}} u_{\mathbf{q}} e^{i\mathbf{q}\cdot\mathbf{r}}, \\ u_{\mathbf{q}} &= \int d\mathbf{r} u(\mathbf{r}) e^{-i\mathbf{q}\cdot\mathbf{r}}. \quad (22) \end{aligned}$$

The impurity-averaged binary potential correlation function is [40]

$$\langle \langle U(\mathbf{r}) U(\mathbf{r}') \rangle \rangle = \frac{1}{\Omega} \sum_{\mathbf{q}} |u_{\mathbf{q}}|^2 n_{\text{imp}} W^2 e^{i\mathbf{q}\cdot(\mathbf{r}-\mathbf{r}')}, \quad (23)$$

where  $n_{\text{imp}}$  is the impurity concentration, and we can see the Fourier component of the averaged correction function is

$w(\mathbf{q}) = |u_{\mathbf{q}}|^2 n_{\text{imp}} W^2$ . To obtain Eq. (20), we need to use the following matrix element,

$$\begin{aligned} |\langle \gamma | e^{i\mathbf{q}\cdot\mathbf{r}} | \gamma' \rangle|^2 &= \Phi_{N_2 N_1} \left( \frac{q_\perp l_B^2}{2} \right) \delta_{k_y, k'_y + q_y} \\ &\times |\langle n_b, k_z | e^{iq_z z} | n'_b, k'_z \rangle|^2, \quad (24) \\ \Phi_{N_2 N_1}(\xi) &= \frac{N_2!}{N_1!} \xi^{N_1 - N_2} e^{-\xi} [L_{N_2}^{N_1 - N_2}(\xi)]^2, \end{aligned}$$

where  $q_\perp = \sqrt{q_x^2 + q_y^2}$ ,  $N_1 = \max(N, N')$ ,  $N_2 = \min(N, N')$ , and  $L_N^\alpha(x)$  is the Laguerre's polynomial. Here, we also assume that the Bloch states are approximated as plane waves and this is proper for a short-range impurity potential and weak periodic potential. For a short-range impurity potential,  $w(\mathbf{q}) \simeq w$  is independent of  $\mathbf{q}$ . In this case, the self-energy in Eq. (20) is independent of  $\gamma$ , and finally we arrive at [40]

$$\Sigma_\varepsilon^s = \frac{w}{2\pi l_B^2} \sum_{N, n_b} \int \frac{dk_z}{2\pi} G_\varepsilon^s(k_z, N, n_b). \quad (25)$$

The density of states (DOS) with level broadening (LB) can be directly evaluated from Eq. (21) by using  $D_{\text{LB}}(\varepsilon) = -g_s \frac{1}{\pi} \sum_{\gamma} \text{Im} G_\varepsilon^+(\gamma)$ . By using Eqs. (21), (25), and (19) it can be transformed into [40]

$$\begin{aligned} \sigma_{xx} = & g_s \frac{e^2 \omega_c}{8\pi^3} \int d\varepsilon \left( -\frac{\partial f(\varepsilon)}{\partial \varepsilon} \right) \frac{(2\Sigma'')^2}{(2\Sigma'')^2 + (\hbar \omega_c)^2} \\ & \times \int dk_z \sum_{n_b, N} \frac{\varepsilon - E_{n_b, k_z} - \Sigma'}{(\varepsilon - E_\gamma - \Sigma')^2 + (\Sigma'')^2}, \quad (26) \end{aligned}$$

and Eq. (19),

$$\begin{aligned} \sigma_{xy} = & \frac{en}{B} - g_s \frac{e^2}{8\pi^3 \hbar} \int d\varepsilon \left( -\frac{\partial f(\varepsilon)}{\partial \varepsilon} \right) \frac{(2\Sigma'')^3}{(2\Sigma'')^2 + (\hbar \omega_c)^2} \\ & \times \int dk_z \sum_{n_b, N} \frac{\varepsilon - E_{n_b, k_z} - \Sigma'}{(\varepsilon - E_\gamma - \Sigma')^2 + (\Sigma'')^2}, \quad (27) \end{aligned}$$

where  $\Sigma'' = \text{Im} \Sigma_\varepsilon^-$ ,  $\Sigma' = \text{Re} \Sigma_\varepsilon^-$ , and

$$n = \int d\varepsilon D_{\text{LB}}(\varepsilon) f(\varepsilon) = \frac{g_s}{\pi w} \int d\varepsilon \Sigma'' f(\varepsilon). \quad (28)$$

Equations (26) and (27) are the main results that we will use later.

### III. CALCULATIONS AND RESULTS FOR KRONIG-PENNEY MODEL

As mentioned above, we have formally described the system. Through the eigensolution of  $h^\parallel$ , energy gaps will emerge in the system with a periodic potential due to the Bragg's diffraction [43]. In order to show a specific result, we start with the Kronig-Penney model with a periodic square-well potential,

$$V(z) = \begin{cases} 0, & nZ < x < nZ + a, \\ V_0, & nZ + a < z < nZ + a + b. \end{cases} \quad (29)$$

Here,  $Z = a + b$  is the barrier period and  $V_0$  is the barrier potential as shown in Fig. 1(a). Using the Bloch theorem

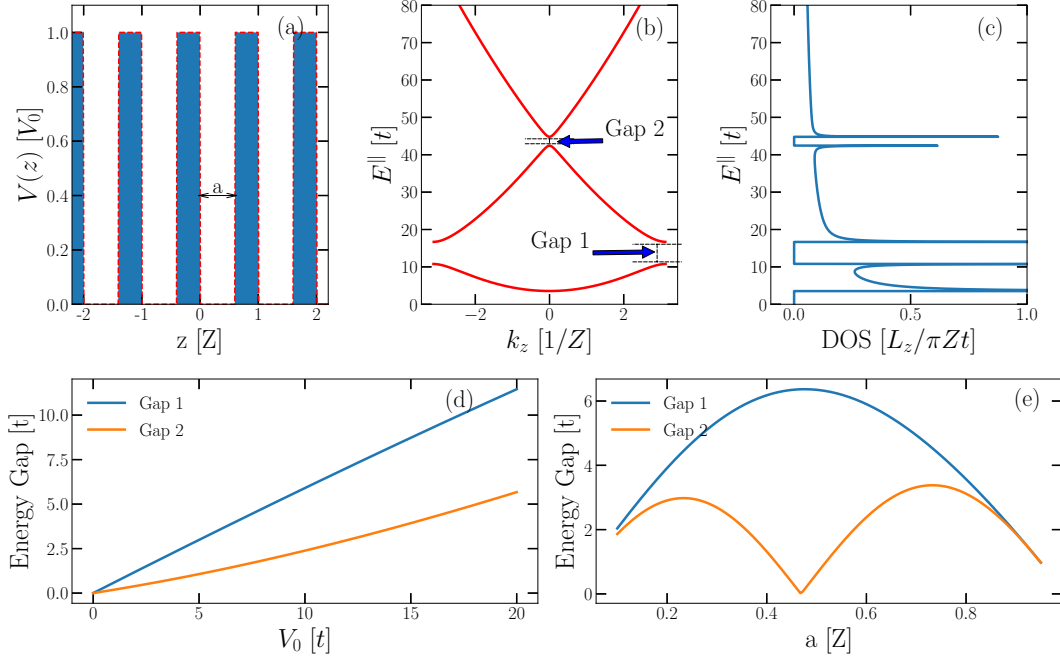


FIG. 1. Properties of the Kronig-Penney model in a 1D periodic potential. (a) The periodic square-well potential defined in Eq. (29). (b) and (c) The Bloch energy spectrum and the corresponding DOS. (d) and (e) The energy gaps as a function of parameters  $V_0$  and  $a$ , respectively. Here, we set  $a/Z = 0.6$ ,  $V_0/t = 10$ , and  $t = \frac{\hbar^2}{2MZ^2}$ .

$f_{k_z}(z + Z) = e^{ik_z Z} f_{k_z}(z)$ , for eigenvalue  $E^{\parallel}$ , we can draw up the eigenfunction

$$f_{k_z}(z) = \begin{cases} Ae^{iKz} + Be^{-iKz}, & 0 < z < a, \\ Ce^{Qz} + De^{-Qz}, & -b < z < 0, \\ [Ce^{Q(z-Z)} + De^{-Q(z-Z)}]e^{ik_z Z}, & a < z < Z, \end{cases} \quad (30)$$

where  $E^{\parallel} = \frac{\hbar^2 K^2}{2M}$  and  $V_0 - E^{\parallel} = \frac{\hbar^2 Q^2}{2M}$ . To get the constant coefficients  $A, B, C, D$ , we utilize the boundary conditions where the wave functions  $f_{k_z}$  and  $df_{k_z}/dz$  are continuous at  $z = 0$  and  $z = a$ , namely,

$$\begin{cases} A + B = C + D, \\ iK(A - B) = Q(C - D), \\ Ae^{iKa} + Be^{-iKa} = (Ce^{-Qb} + De^{Qb})e^{ik_z Z}, \\ iK(Ae^{iKa} - Be^{-iKa}) = Q(Ce^{-Qb} - De^{Qb})e^{ik_z Z}. \end{cases} \quad (31)$$

Equation (31) has nontrivial solutions only if the determinant of the coefficients' matrix vanishes, yielding

$$\frac{Q^2 - K^2}{2QK} \sinh Qb \sin Ka + \cosh Qb \cos Ka = \cos k_z Z. \quad (32)$$

Numerically solving Eq. (32), we learn the energy dispersion relations between  $E_{nb, k_z}^{\parallel}$  and  $k_z$  in the first Brillouin zone as depicted in Fig. 1(b). More clearly, the first two energy gaps have been displayed in Figs. 1(d) and 1(e).

As for the density of states (DOS) of the Bloch bands, denoting the left and right sides of Eq. (32) as  $f_{\text{LHS}}(E^{\parallel})$  and  $f_{\text{RHS}}(k_z)$ , respectively, and taking the derivative of both sides

of Eq. (32), we can calculate the DOS numerically by

$$D^{\parallel}(E^{\parallel}) \equiv \frac{L_z}{2\pi} \frac{dk_z}{dE^{\parallel}} = \frac{L_z}{\pi Z} \frac{|f'_{\text{LHS}}(E^{\parallel})|}{\sqrt{1 - f_{\text{LHS}}^2(E^{\parallel})}}, \quad (33)$$

where  $f'_{\text{LHS}}(E^{\parallel}) = df_{\text{LHS}}/dE^{\parallel}$ , which is plotted in Fig. 1(c). Next, we will study the system described by Hamiltonian  $H_0$ . From the simultaneous equations (7) and (32), we obtain the energy bands as plotted in Fig. 2(a). The Hall conductivity from Eq. (11) has been calculated for different Fermi levels and magnetic fields as shown in Fig. 2(b). Making Eq. (33) go further, we can get the DOS,

$$D(E) = \frac{L_x L_y}{2\pi l_B^2} \sum_N D^{\parallel} \left[ E - \left( N + \frac{1}{2} \right) \hbar \omega_c \right]. \quad (34)$$

The Hall conductivity and the corresponding DOS have been collected in Figs. 2(c) and 2(d).

By using Eqs. (21) and (25)–(27), TMC and Hall conductivities can be evaluated due to LB. Furthermore, the magnetoresistivities are calculated with the relations

$$\rho_{xx} = \frac{\sigma_{xx}}{\sigma_{xx}^2 + \sigma_{xy}^2}, \quad (35)$$

and

$$\rho_{xy} = \frac{\sigma_{xy}}{\sigma_{xx}^2 + \sigma_{xy}^2}. \quad (36)$$

The results of magnetoresistivities  $\rho_{xx}$  and  $\rho_{xy}$  varying with magnetic field are shown in Fig. 3. For a large periodic potential or high Fermi level, 3D QHE remains robust against impurities. However, when the periodic potential is small and the Fermi energies are low,  $\rho_{xx}$  and  $\rho_{xy}$  become subtle.

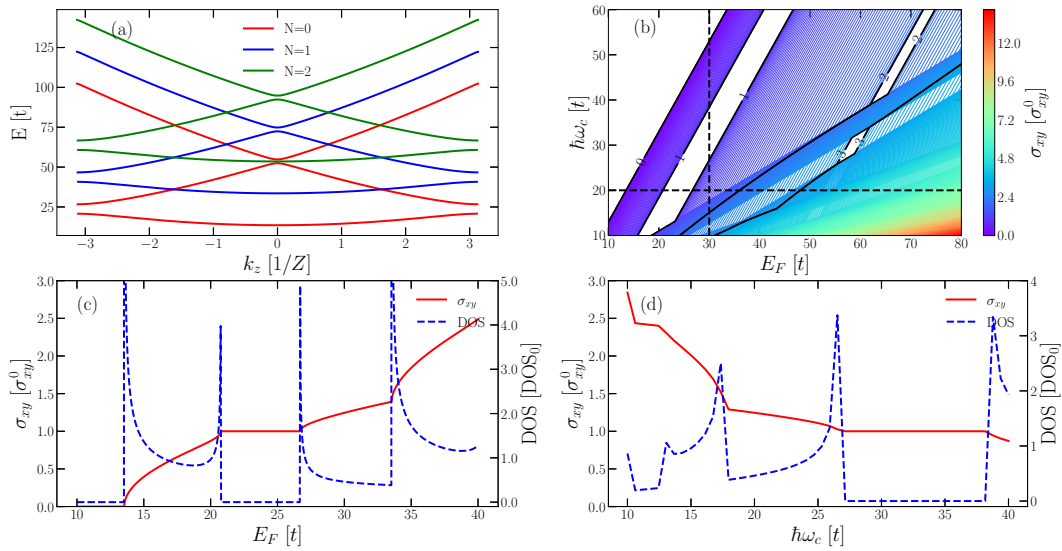


FIG. 2. Results of Landau level, Hall conductivity, and corresponding DOS. (a) The energy spectrum includes three Landau levels that are plotted where we take  $\hbar\omega_c/t = 20$ . (b) The contour lines of Hall conductivity in units of  $\sigma_{xy}^0$  with varying  $\hbar\omega_c$  and Fermi level  $E_F$ . The Hall plateaus lie exactly in the blank white space enclosed by black solid contour lines and the numbers 0, 1, 2, 3 superimposed on the black solid contour lines denote the quantized values of Hall conductivity. The Hall conductivity and the corresponding DOS in units of  $\text{DOS}_0$  as a function of (c)  $E_F$  for  $\hbar\omega_c/t = 20$  and (d)  $\hbar\omega_c$  for  $E_F/t = 30$ . The black dashed lines in (b) correspond to the cross sections in (c) and (d). Here, we set  $\sigma_{xy}^0 = g_s \frac{e^2}{2\pi h} \frac{2\pi}{Z}$ ,  $\text{DOS}_0 = \frac{\Omega}{\pi Z^3 t}$ , and the other parameters are the same as in Fig. 1.

#### IV. DISCUSSION AND CONCLUSION

Now we will discuss the above results. First, as is revealed in Fig. 1(b), the energy gap can be opened when a periodic potential is applied in the  $z$  direction. As the “strength” of the square-well potential increases, the gaps increase linearly, as Fig. 1(d) depicts. Interesting, what Fig. 1(e) presents is that the gaps may reach an extreme value when the width of the square-well potential is about half of its period  $Z$ .

In Fig. 2(a), we can see that when the parameters  $V_0$ ,  $a$ , and  $B$ , are chosen properly, the second Landau band may above the energy appear in Bloch bands in the first Landau band, which means robust Hall plateaus may appear. In Fig. 2(b), we take the time to search for the places where the plateaus may appear by modulating the Fermi energy and magnetic field. From this figure, we find that there will be Hall plateaus in the blank region enclosed by the black solid contour lines. It is also possible that two plateaus appear when the magnetic field and Fermi energy are both large enough. Figures 2(c) and 2(d) visualize the correspondence very well. The DOS vanishes when a Hall plateau appears. From the oscillating DOS, we can infer that there exist similar oscillations of TMCs.

Besides manifesting the existence of the 3D QHE, the effect of the impurities has to be taking into consideration. As impurities are unavoidable experimentally, they have non-negligible effects on transverse magnetotransport, which is in fact a scattering-associated process. In Figs. 3(a) and 3(b), we show the information of the spectrum and Fermi energies, which correspond to Figs. 3(c)–3(f), respectively. Figures 3(c)–3(f) show the TMRs  $\rho_{xx}$  and Hall resistivities  $\rho_{xy}$  varying with magnetic field  $B$  by taking different impurity strengths. All the results in Figs. 3(c)–3(f) are calculated to quantum limit regimes. First, from the results we can see that the minimum TMRs  $\rho_{xx}$  always show up in the quantum limit,

and this result tells us the finite minimum TMRs  $\rho_{xx}$  cannot be used as a unique signature of 3D QHE as been observed in recent experiments [30–32,34]. Second, Figs. 3(c)–3(f) show that  $\rho_{xx}$  will increase as the impurities increase, and this indicates that the minimum TMRs  $\rho_{xx}$  will become finite as the impurities increase when the periodic potential is not so strong. In Figs. 3(c)–3(e) the energy spectrum remains the same with different typical Fermi energies. In Fig. 3(c), we take the Fermi energy being slightly below the energy gap in the first Bloch band. In this case, the TMRs and Hall resistivities show similar signatures when comparing to the normal 3D electron gas in a magnetic field. In this regime, the so-called QHE appears [34], and as the impurities become stronger, the quasiquantized plateaus become more quantized in the quantum limit, but also the TMRs will become larger. Figure 3(d) shows even more interesting results where we take the Fermi energy slightly above the energy gap in the second Bloch band. The quantized Hall plateaus do not appear, which is not so obvious physically. In this case only QHE appears, and it is hard to distinguish between the cases of a periodic system and a normal 3D electron gas as in Fig. 3(c). This result makes the case even more complex so that the answer to whether or not 3D QHE can be properly observed experimentally in the periodic system becomes unclear. When the Fermi energy increases further, the 3D QHE will emerge, and will be robust to weak impurities. But even in this regime, the situation becomes subtle when the impurities become strong enough as depicted in Fig. 3(e) when  $w/w_0 = 4.0$ . The quantized plateau will evolve into a slope and vanishing TMRs become finite. This can be understood as an effect of level broadening. In fact, the level broadening  $\bar{\epsilon}$  due to the impurities has a close relation with  $w$ , and it can be expressed as [44]  $\bar{\epsilon} = \hbar/\tau_{sc} = \pi w D_{LB}$ . After some calculation, we can

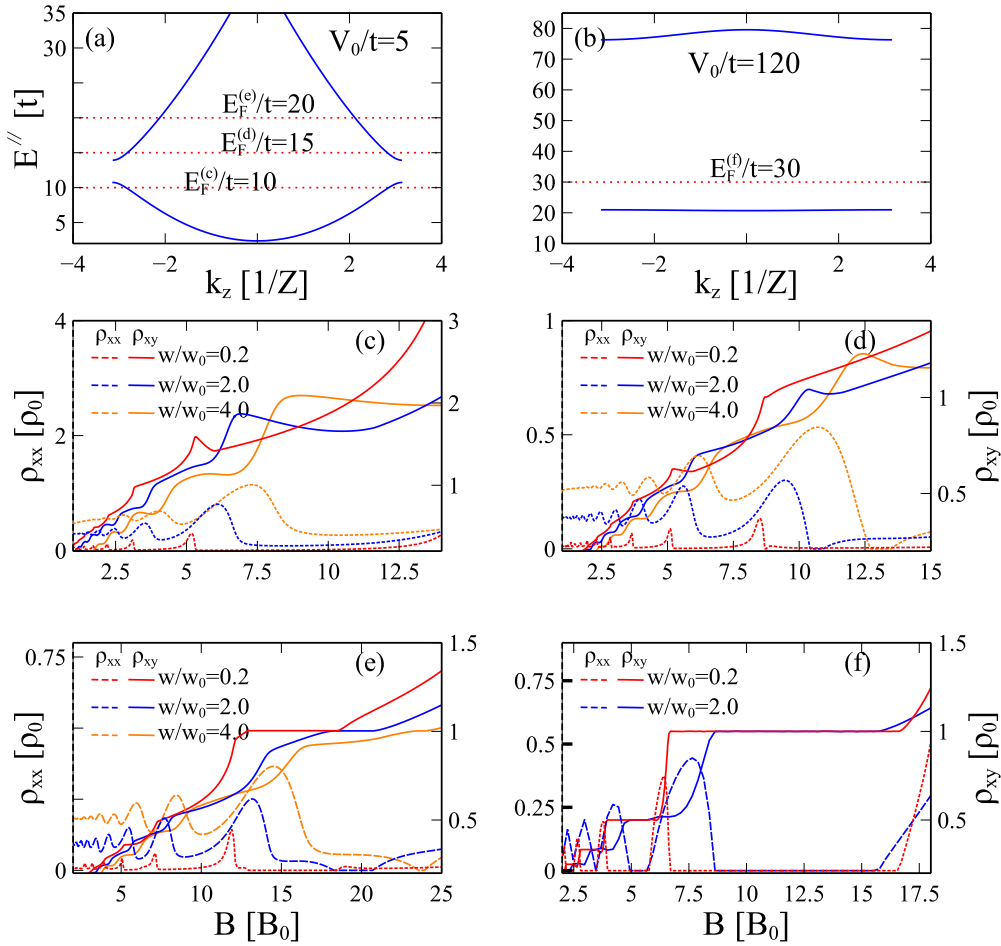


FIG. 3. Influence of the white noise impurities on the Hall resistivities and the TMRs. (a) and (b) show the energy spectrum along the  $z$  direction given by different periodic potentials  $V_0$ . In (a),  $V_0/t = 5$ ,  $a/Z = 0.5$ , and  $E_F^{(c)-(e)}$  correspond to the Fermi energies used in (c)–(e), respectively. In (b),  $V_0/t = 120$ ,  $a/Z = 0.5$ , and  $E_F^{(f)}$  correspond to the Fermi energy used in (f). (c)–(f) show the magnetoresistivities  $\rho_{xx}$  and  $\rho_{xy}$ , varying with magnetic field  $B$  at different disorder strengths  $w/w_0$  with  $w_0 = t^2 Z^3$ . The left y axis represents  $\rho_{xx}$  and the right y axis represents  $\rho_{xy}$ . Here, we denote  $\rho_0 = \frac{h}{e^2} \frac{Z}{g_s}$ , and  $B_0 = \frac{Mt}{\hbar e}$ .

estimate that  $\bar{\epsilon}/t \sim 5$  at  $w/w_0 \sim 4$ , and the magnitude of the gap  $\delta E/t \sim 5$ . In Fig. 3(d), we refer to these regimes as low Fermi energy regimes, and the QHE appear just because the initial Fermi energy is low. In Fig. 3(e), the disappearance of 3D QHE is due to the strong impurities compared to the energy gap.

In Fig. 3(f), we take a large periodic potential  $V_0$  and the results are similar to those of the bulk Hall effect in the artificial superlattice system in Ref. [29]. As a matter of fact, the parameters used here are mainly estimated from those in Ref. [29], and we find the artificial superlattice is more likely to construct a larger layer periodic barrier potential. From our results, we see that the larger periodic potential will result in a larger energy gap and more robust 3D QHE. This makes the artificial superlattice an ideal platform for engineering and studying 3D QHE compared with the natural materials in which the spontaneous periodic potential is probably weak.

From the above discussions and results, we conclude that in a periodic system with either a CDW- or SDW-type or superlattice-type periodic potential, the 3D QHE can appear by tuning the system parameters properly. A more detailed

study shows that distinguishing between QHE and 3DQHE is not so clear just from the signatures of TMRs and Hall resistivities. The finite minimum values of  $\rho_{xx}$  together with quasiquantized Hall plateaus can emerge from four different cases. The first one is the normal 3D electron gas without impurities in the vicinity of the quantum limit as shown in Ref. [34]. The second one is a multiband explanation as argued in Refs. [31,32]. We show two mechanisms, which are the “low” Fermi energy mechanism when the Fermi energy is in or slightly above the Bloch gap and the “strong” impurity effect when the LL broadening is comparable with the Bloch band gap. According to our conclusions, maybe other experimental methods should be considered to ascertain whether spontaneous periodicity exists in the system, such as performing a scanning tunneling measurement (STM) on the surface of the  $x$ - $z$  or  $y$ - $z$  plane to search for the periodic CDWs, etc. Also, we argue that the artificial superlattice can be engineered to be an ideal platform for studying 3D QHE properties, as the large layer barrier periodic potential can be manually fabricated.

The code and data used to produce the figures are available online [45].

## ACKNOWLEDGMENTS

We appreciate useful discussions with R. Ma and W. Luo. This work was supported by the State Key Program for Basic Researches of China under Grant No.

2017YFA0303203 (D.Y.X.), and the National Natural Science Foundation of China under Grant No. 11974168 (L.S.). H.G. and G.Y.Q. contributed equally to this work.

- 
- [1] K. v. Klitzing, G. Dorda, and M. Pepper, *Phys. Rev. Lett.* **45**, 494 (1980).
- [2] D. C. Tsui, H. L. Stormer, and A. C. Gossard, *Phys. Rev. Lett.* **48**, 1559 (1982).
- [3] Y. Zhang, Y.-W. Tan, H. L. Stormer, and P. Kim, *Nature (London)* **438**, 201 (2005).
- [4] M. Z. Hasan and C. L. Kane, *Rev. Mod. Phys.* **82**, 3045 (2010).
- [5] X.-L. Qi and S.-C. Zhang, *Rev. Mod. Phys.* **83**, 1057 (2011).
- [6] N. P. Armitage, E. J. Mele, and A. Vishwanath, *Rev. Mod. Phys.* **90**, 015001 (2018).
- [7] D. J. Thouless, M. Kohmoto, M. P. Nightingale, and M. den Nijs, *Phys. Rev. Lett.* **49**, 405 (1982).
- [8] S. T. Hannahs, J. S. Brooks, W. Kang, L. Y. Chiang, and P. M. Chaikin, *Phys. Rev. Lett.* **63**, 1988 (1989).
- [9] J. R. Cooper, W. Kang, P. Auban, G. Montambaux, D. Jérôme, and K. Bechgaard, *Phys. Rev. Lett.* **63**, 1984 (1989).
- [10] S. Hill, S. Uji, M. Takashita, C. Terakura, T. Terashima, H. Aoki, J. S. Brooks, Z. Fisk, and J. Sarrao, *Phys. Rev. B* **58**, 10778 (1998).
- [11] H. Cao, J. Tian, I. Miotkowski, T. Shen, J. Hu, S. Qiao, and Y. P. Chen, *Phys. Rev. Lett.* **108**, 216803 (2012).
- [12] H. Masuda, H. Sakai, M. Tokunaga, Y. Yamasaki, A. Miyake, J. Shiozai, S. Nakamura, S. Awaji, A. Tsukazaki, H. Nakao *et al.*, *Sci. Adv.* **2**, e1501117 (2016).
- [13] Y. Xu, I. Miotkowski, C. Liu, J. Tian, H. Nam, N. Alidoust, J. Hu, C.-K. Shih, M. Z. Hasan, and Y. P. Chen, *Nat. Phys.* **10**, 956 (2014).
- [14] C. M. Wang, H.-P. Sun, H.-Z. Lu, and X. C. Xie, *Phys. Rev. Lett.* **119**, 136806 (2017).
- [15] H.-Z. Lu, *Natl. Sci. Rev.* **6**, 208 (2019).
- [16] G.-Q. Zhao, W. Rui, C. Wang, H.-Z. Lu, and X. Xie, [arXiv:2004.01386](https://arxiv.org/abs/2004.01386).
- [17] B. I. Halperin, *Jpn. J. Appl. Phys.* **26**, 1913 (1987).
- [18] V. Celli and N. D. Mermin, *Phys. Rev.* **140**, A839 (1965).
- [19] A. H. MacDonald, *Phys. Rev. B* **37**, 4792 (1988).
- [20] Y. Takada and H. Goto, *J. Phys.: Condens. Matter* **10**, 11315 (1998).
- [21] J. T. Chalker, in *Supersymmetry and Trace Formulae*, edited by I. V. Lerner, J. P. Keating, and D. E. Khmel'nitskii, NATO Advanced Studies Institute, Series B: Physics, Vol. 370 (Springer, Boston, 1999), pp. 75–83.
- [22] F. J. Burnell, B. A. Bernevig, and D. P. Arovas, *Phys. Rev. B* **79**, 155310 (2009).
- [23] K. Akiba, A. Miyake, H. Yaguchi, A. Matsuo, K. Kindo, and M. Tokunaga, *J. Phys. Soc. Jpn.* **84**, 054709 (2015).
- [24] M. Kohmoto, B. I. Halperin, and Y.-S. Wu, *Phys. Rev. B* **45**, 13488 (1992).
- [25] B. A. Bernevig, T. L. Hughes, S. Raghu, and D. P. Arovas, *Phys. Rev. Lett.* **99**, 146804 (2007).
- [26] M. Koshino and H. Aoki, *Phys. Rev. B* **67**, 195336 (2003).
- [27] L. Balents and M. P. A. Fisher, *Phys. Rev. Lett.* **76**, 2782 (1996).
- [28] J. T. Chalker and A. Dohmen, *Phys. Rev. Lett.* **75**, 4496 (1995).
- [29] H. L. Störmer, J. P. Eisenstein, A. C. Gossard, W. Wiegmann, and K. Baldwin, *Phys. Rev. Lett.* **56**, 85 (1986).
- [30] F. Tang, Y. Ren, P. Wang, R. Zhong, J. Schneeloch, S. A. Yang, K. Yang, P. A. Lee, G. Gu, Z. Qiao, and L. Zhang, *Nature (London)* **569**, 537 (2019).
- [31] P. Wang, Y. Ren, F. Tang, P. Wang, T. Hou, H. Zeng, L. Zhang, and Z. Qiao, *Phys. Rev. B* **101**, 161201(R) (2020).
- [32] S. Galeski, X. Zhao, R. Wawrzyńczak, T. Meng, T. Förster, P. M. Lozano, S. Honnali, N. Lamba, T. Ehmcke, A. Markou, Q. Li., G. Gu, W. Zhu, J. Wosnitzer, C. Felser, G. F. Chen, and J. Gooth, *Nat. Commun.* **11**, 5926 (2020).
- [33] F. Qin, S. Li, Z. Z. Du, C. M. Wang, W. Zhang, D. Yu, H.-Z. Lu, and X. C. Xie, *Phys. Rev. Lett.* **125**, 206601 (2020).
- [34] S. Galeski, T. Ehmcke, R. Wawrzyńczak, P. M. Lozano, K. Cho, A. Sharma, S. Das, F. Küster, P. Sessi, M. Brando, R. Küchler, A. Markou, M. König, P. Swekis, C. Felser, Y. Sassa, Q. Li, G. Gu, M. V. Zimmermann, O. Ivashko *et al.*, *Nat. Commun.* **12**, 3197 (2021).
- [35] L. Landau, E. Lifshitz, and J. Sykes, *Non-relativistic Theory. Quantum Mechanics*, Course of Theoretical Physics (Butterworth-Heinemann, Oxford, U.K., 1998).
- [36] K. Ziegler, *Phys. Rev. Lett.* **97**, 266802 (2006).
- [37] K. Chadova, Electronic transport within the Kubo-Bastin formalism, Dissertation, LMU München, 2017, <https://edoc.ub.uni-muenchen.de/21609/>.
- [38] A. Bastin, C. Lewiner, O. Betbeder-matibet, and P. Nozieres, *J. Phys. Chem. Solids* **32**, 1811 (1971).
- [39] E. N. Economou, Time-independent Green's functions, *Green's Functions in Quantum Physics*, Springer Series in Solid-State Sciences Vol. 7 (Springer, Berlin, 2006), pp. 3–19.
- [40] F. T. Vasko and O. E. Raichev, Quantum magnetotransport, *Quantum Kinetic Theory and Applications: Electrons, Photons, Phonons* (Springer, New York, 2005), pp. 425–482.
- [41] T. Ando and Y. Uemura, *J. Phys. Soc. Jpn.* **36**, 959 (1974).
- [42] T. Ando, *J. Phys. Soc. Jpn.* **37**, 1233 (1974).
- [43] C. Kittel and P. McEuen, *Introduction to Solid State Physics* (Wiley, New York, 1976), Vol. 8.
- [44] F. T. Vasko and O. E. Raichev, Electron-impurity system, in *Quantum Kinetic Theory and Applications: Electrons, Photons, Phonons* (Ref. [40]), pp. 51–98.
- [45] <https://doi.org/10.5281/zenodo.5524768>.